Applied Physics Letters

Scalability of multi-junction organic solar cells for large area organic solar modules

Cite as: Appl. Phys. Lett. **106**, 213301 (2015); https://doi.org/10.1063/1.4921771
Submitted: 09 March 2015 • Accepted: 15 May 2015 • Published Online: 28 May 2015

Xin Xiao, Kyusang Lee and Stephen R. Forrest

AIP Publishing

Scalability of multi-junction organic solar cells for large area organic solar modules

Xin Xiao,[1] Kyusang Lee,[1] and Stephen R. Forrest[1,2]
[1]*Department of Electrical Engineering and Computer Science, University of Michigan, Ann Arbor, Michigan 48109, USA*
[2]*Departments of Physics and Materials Science and Engineering, University of Michigan, Ann Arbor, Michigan 48109, USA*

(Received 9 March 2015; accepted 15 May 2015; published online 28 May 2015)

We investigate the scalability of multi-junction organic photovoltaic cells (OPV) with device areas ranging from 1 mm^2 to 1 cm^2, as well as 25 cm^2 active area solar modules. We find that the series resistance losses in 1 cm^2 *vs.* 1 mm^2 OPV cell efficiencies are significantly higher in single junction cells than tandem, triple, and four junction cells due to the lower operating voltage and higher current of the former. Using sub-electrodes to reduce series resistance, the power conversion efficiency (*PCE*) of multi-junction cells is almost independent of area from 1 mm^2 to 1 cm^2. Twenty-five, 1 cm^2 multi-junction cell arrays are integrated in a module and connected in a series-parallel circuit configuration. A yield of 100% with a deviation of *PCE* from cell to cell of $<10\%$ is achieved. The module generates an output power of 162 ± 9 mW under simulated AM1.5G illumination at one sun intensity, corresponding to $PCE = 6.5 \pm 0.1\%$, slightly lower than *PCE* of discrete cells ranging from 6.7% to 7.2%. © *2015 AIP Publishing LLC*. [http://dx.doi.org/10.1063/1.4921771]

The power conversion efficiency (*PCE*) of organic photovoltaic cells (OPV) has increased substantially over the past few years.[1–11] Particularly, it has been demonstrated that multi-junction OPV cells can achieve higher *PCE* than single junction cells due to reduced thermalization losses and broadened coverage of the solar spectrum.[4–6] There is, however, less attention paid to scaling the size of OPV cells, particularly those consisting of more than one active cell in a stack (i.e., multi-junction cells), which is key for their practical application.[12–17] Here, we report on a systematic investigation of the scalability of multi-junction OPV cells ranging from 1 mm^2 to 1 cm^2, and find the reduction in *PCE* with increased active area is due to increased indium tin oxide (ITO) anode series resistance, which in turn reduces the fill factor (*FF*). Further, multi-junction OPV cells show reduced losses with cell area compared to single-junction cells due to their higher open-circuit voltage (V_{OC}) and lower short-circuit current density (J_{SC}). Based on our findings, we fabricated OPV modules comprised of an array of 25, 1 cm^2 multi-junction cells. A yield of 100% for the discrete cells in the array is achieved across the module, with a variation of *PCE* from cell-to-cell of $<10\%$. The OPV module generates an electrical power of 162 ± 9 mW under simulated AM1.5G illumination at one sun intensity, corresponding to $PCE = 6.5 \pm 0.1\%$.

We studied the scalability of single, tandem, triple, and four junction OPV cells based on the donors, 2-((7-(5-(di-p-tolylamino)thiophen-2-yl)benzo[c][1,2,5]thiadiazol-4yl) methylene) malononitrile (DTDCTB), and tetraphenyldibenzoperiflanthene (DBP) combined with C_{60} and C_{70} acceptors. In multi-junction structures, a DBP:C_{70} planar-mixed heterojunction (PM-HJ) is employed as a blue-green absorbing sub-cell (sub-cell 1, SC1, in Fig. 1) while the DTDCTB:C_{60} PM-HJ primarily absorbs in the near-infrared (SC2 in Fig. 1). For multilayer devices, sub-cells were interconnected with a charge generation layer (CGL) comprising bathophenanthroline (BPhen):C_{60} mixed layer (5 nm, 1:1 vol. ratio)/Ag (0.1 nm)/MoO_3 (5 nm). Four-junction cells consist of the following structure (from the cathode): Ag (100 nm)/BPhen (7 nm)/SC1/CGL/SC2/CGL/SC1/CGL/SC2/MoO_3 (10 nm)/ITO. For triple, tandem, and single junction cells, the sub-cells and CGLs closest to the anode are eliminated according to the number of stages (e.g., a tandem has active regions of SC1/CGL/SC2). Each device structure is optimized through both experiments and simulations.[6]

The OPV cells were grown on glass substrates pre-coated with ITO with a sheet resistance of 15 Ω/sq. We obtained all source chemicals from commercial suppliers: DBP, DTDCTB, and BPhen (Lumtec), C_{70} (SES Research), C_{60} (MER), and MoO_3 (Alfa Aesar). The substrates were sonicated in detergent and a series of organic solvents including acetone and isopropanol for 10 min each. After solvent cleaning, the substrates were snow-cleaned[18] to remove large particles, and subsequently exposed to ultra-violet ozone for 10 min immediately prior to loading in a high vacuum chamber with a base pressure of 10^{-7} Torr for the deposition of organic layers. Then, 100 nm-thick Al cathodes were deposited through shadow masks. The device areas were defined as the overlap area between the ITO anode and metal cathode. Completed devices were transferred in a high-purity N_2-filled glovebox with <0.1 ppm O_2 and H_2O without exposure to ambient air for the current density-voltage (*J-V*) measurement in the dark and under simulated AM 1.5G illumination.

Device performance as a function of area is shown in Fig. 2 and Table I for single, double, triple, and four junction cells. The higher *PCE* of multi-junction compared with single junction cells results from a broadened coverage of the solar spectrum and reduced thermalization losses.[4,6,19] While J_{SC} and V_{OC} of each device type remains almost the same as

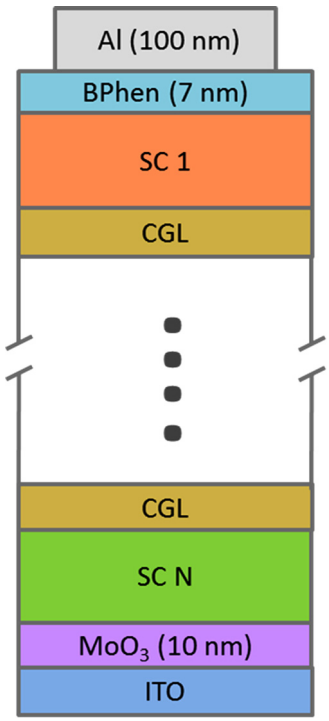

FIG. 1. Schematic of a multi-junction organic photovoltaic (OPV) cell. Single junction cells have photoactive layers of DBP:C_{70} (54 nm, 1:8 vol. ratio)/C_{70} (9 nm). For multi-junction cells, the structures of sub-cell 1 (SC1) and sub-cell 2 (SC2) are DBP:C_{70} (30 nm, 1:8 vol. ratio)/C_{70} (7 nm) and DTDCTB:C_{60} (60 nm, 1:1 vol. ratio)/C_{60} (5 nm), respectively. Sub-cells are connected with charge generation layers (CGL) consisting of BPhen:C_{60} mixed layer (5 nm, 1:1 vol. ratio)/Ag (0.1 nm)/MoO_3 (5 nm). Four-junction cells consist of the following structure (from the cathode): Ag (100 nm)/BPhen (7 nm)/SC1/CGL/SC2/CGL/SC1/CGL/SC2/MoO_3 (10 nm)/ITO. For triple and tandem cells, the sub-cells and CGLs closest to the anode are eliminated according to the number of stages.

TABLE I. Device performance of single, tandem, triple, and four junction OPV cells with different device areas.

Device (area)	J_{SC} (mA/cm^2)	V_{OC} (V)	*FF*	*PCE* (%)
Single (1 mm^2)	11.3 ± 0.2	0.92 ± 0.01	0.59 ± 0.01	6.1 ± 0.2
Single (1 cm^2)	11.3 ± 0.2	0.91 ± 0.01	0.49 ± 0.01	5.0 ± 0.2
Tandem (1 mm^2)	7.5 ± 0.2	1.70 ± 0.02	0.58 ± 0.01	7.4 ± 0.2
Tandem (1 cm^2)	7.5 ± 0.2	1.69 ± 0.02	0.53 ± 0.01	6.7 ± 0.2
Triple (1 mm^2)	5.3 ± 0.1	2.59 ± 0.02	0.58 ± 0.01	8.0 ± 0.2
Triple (1 cm^2)	5.3 ± 0.1	2.59 ± 0.02	0.54 ± 0.01	7.5 ± 0.2
Four (1 mm^2)	4.7 ± 0.1	3.34 ± 0.02	0.57 ± 0.01	8.9 ± 0.2
Four (1 cm^2)	4.6 ± 0.1	3.33 ± 0.02	0.54 ± 0.01	8.3 ± 0.2

a function of device area (Figs. 2(a) and 2(b)), *FF* decreases as area increases (Fig. 2(c)). Among various devices, single junction cells exhibit the largest drop of 17.2 ± 1.7% in *PCE* as area increases from 1 mm^2 to 1 cm^2, whereas tandem, triple, and four junction cells suffer reductions of 8.5 ± 0.8%, 6.3 ± 0.6%, and 4.1 ± 0.5%, respectively. The reduced loss in multi-junction cells is primarily due to increased V_{OC} and reduced J_{SC} with each additional element.

To understand the effect of scaling on device performance, the specific series resistance (R_SA) of the OPV cells was analyzed as a function of device area (A). Thus, we can write[12]

$$R_SA = R_{sheet}\left(\frac{L}{W}\right)A + \sum_N (\rho_{org}t_{org} + r_{int}), \qquad (1)$$

where the sum is over each element in the stacked device consisting of $N = 1$, 2, 3, or 4 sub-elements, R_{sheet} is the sheet resistance of ITO, L and W are the length and width of the ITO contact, ρ_{org} is the resistivity of the organic layer, t_{org} is the thickness of organic layer, and r_{int} is the specific interface

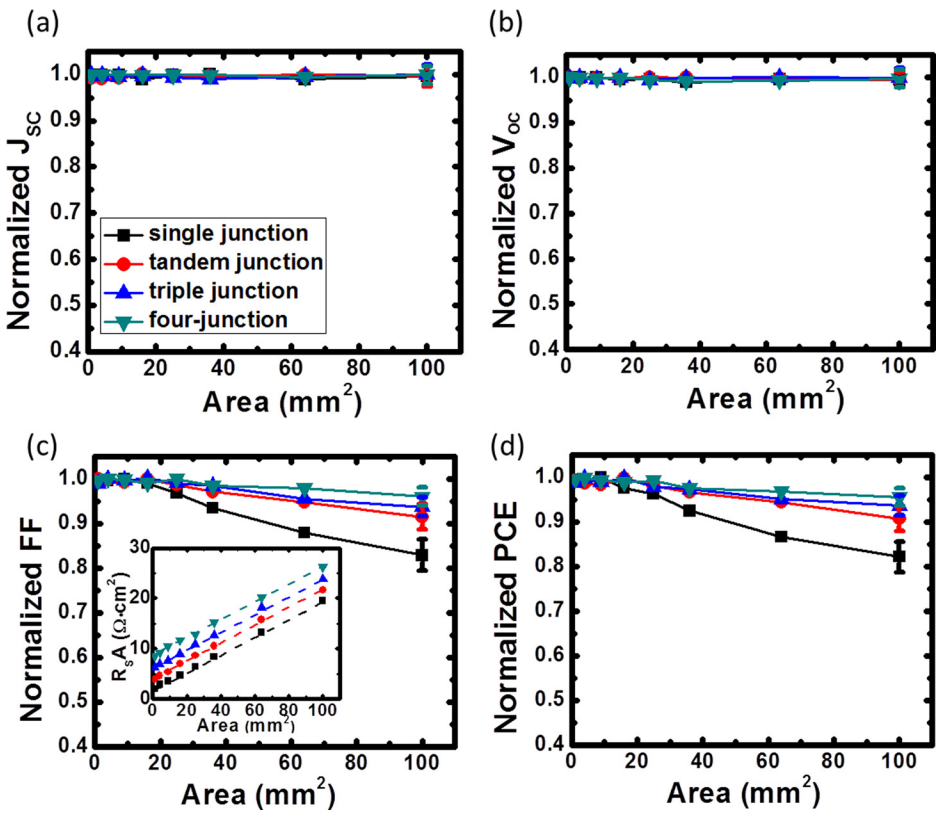

FIG. 2. Normalized device performance (a) short circuit current density, J_{SC}, (b) open circuit voltage, V_{OC}, (c) fill factor, *FF*, and (d) power conversion efficiency, *PCE*, as functions of area for single, tandem, three, and four-junction OPVs. Inset of (c): series resistance *vs.* device area. Actual efficiencies of each device with 1 mm^2 and 1 cm^2 area are provided in Table I.

resistance. The term of $R_{sheet}(L/W)A$ corresponds to the contribution from ITO which results from charge transport across the anode, while $\sum_N(\rho_{org}t_{org} + r_{int})$ corresponds to the contribution from the organic layers and interfaces. This can be approximated as

$$R_SA = R_{sheet}\left(\frac{L}{W}\right)A + N \times r_{jn}, \tag{2}$$

where r_{jn} is the specific resistance of organic layers and interfaces for a single junction. We obtain R_SA from a fit to the ideal dark current density-voltage (J-V) characteristics described using[20]

$$J(V) \approx J_s\left[\exp\left(q\frac{[V - J \cdot R_SA]}{nk_BT}\right) - \chi\right] - J_{ph}(V), \tag{3}$$

where J_s is the saturation current density in the dark, n is the ideality factor associated with the donor (acceptor) layer, k_B is the Boltzmann constant, T is the temperature, q is the elementary charge, and J_{ph} is the photocurrent density. Also, $\chi \sim 1$ is the ratio of the polaron-pair dissociation rate at the heterojunctions between donor and acceptor at V to its value at equilibrium ($V = 0$). As shown in the inset of Fig. 2(c), R_SA increases linearly with device area, as expected. From Eq. (2), a fit to the data gives the average junction resistance $\overline{r_{jn}} = 2.1 \pm 0.2\ \Omega\ \text{cm}^2$. For the $1\,\text{mm}^2$ single junction cell, $R_{sheet}A = 0.015 \pm 0.002\ \Omega\ \text{cm}^2$, which is small compared with $r_{jn} = 1.90 \pm 0.08\ \Omega\ \text{cm}^2$. However, for the $1\,\text{cm}^2$ single junction cell, $R_{sheet}A$ increases to $18 \pm 1\ \Omega\ \text{cm}^2$ which is now dominant. Multi-junction cells show a similar trend as the single-junction cell. However, since the organic contribution is higher for multi-junction OPV cells due to more organic layers and interfaces, scaling of resistance with area is not as pronounced as for single junction OPVs, and hence the ITO sheet resistance plays a relatively small role in multi-junction cells compared to contributions from R_{jn}, while for large area cells, ITO resistance dominates, leading to a significant drop in FF and, therefore, PCE.

To further understand the area dependence of FF, we write[21]

$$\frac{FF(R_SA)}{FF(0)} = 1 - \left(\frac{J_{SC}R_SA}{V_{OC}}\right), \tag{4}$$

where $FF(0)$ is the fill factor at $R_SA = 0$. The normalized FF in Eq. (4) as a function of J_{SC} and V_{OC} is shown in Fig. 3. For comparison, we fix R_SA at the value for single junction cells to focus on the influence of J_{SC} and V_{OC} on FF. Note, R_SA is dominated by the ITO series resistance for $1\,\text{cm}^2$ devices, independent of N. Therefore, the single junction cell has the largest loss in FF due to its higher J_{SC} and lower V_{OC}. The tandem cell has almost double the V_{OC} and half J_{SC} compared to single junction cells, leading to a significantly reduced loss in FF. Similarly, triple and four junction cells exhibit proportionately higher V_{OC} and lower J_{SC} and an even smaller FF loss, which is less than 5% for $N = 4$. The experimental results (Fig. 2(c)) are in agreement with calculations (stars in Fig. 3). Multi-junction cells with area $>1\,\text{cm}^2$ should follow the same trend as shown.

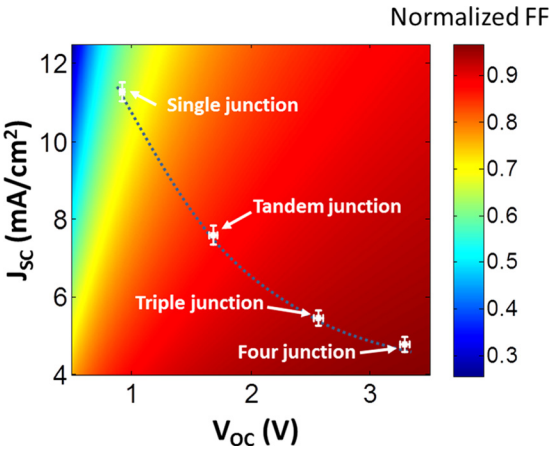

FIG. 3. Calculated normalized FF as a function of J_{SC} and V_{OC}. The stars represent the measured coordinates of OPV cells with different stacking arrangements that are in agreement with calculation. The dashed line serves as a guide to the eye.

To reduce the dominant contribution to R_SA from ITO, we employ a sub-electrode structure[22] with our tandem cells. The sub-electrodes consist of a metal bus bar around 95% of the device perimeter, thereby reducing R_SA to $7.2 \pm 0.3\ \Omega\ \text{cm}^2$ compared to $21.6 \pm 1.3\ \Omega\ \text{cm}^2$ for a $1\,\text{cm}^2$ cell without sub-electrodes. The reduced series resistance improves FF from $53 \pm 1\%$ to $58 \pm 1\%$, thus leading to an increase in PCE from $6.7 \pm 0.2\%$ to $7.3 \pm 0.2\%$, which is almost the same as the efficiency of small-area cells with an identical device structure.

With this understanding of scalability, we fabricated a module comprised of 25, $1\,\text{cm}^2$ discrete tandem cells as shown in Fig. 4. For each discrete cell, the sub-electrode is employed to reduce the series resistance from the anode. Five discrete cells are connected in series to form a column, while five columns are connected in parallel to form a module in Fig. 4(b). A photograph of a complete module is shown in the inset of Fig. 5(b).

OPV modules were fabricated on glass substrates. First, ITO was sputtered through a shadow mask in a high vacuum chamber with a base pressure of 1×10^{-7} Torr. Then, the ITO/glass substrates were cleaned as above. Organic layers and metal contacts (including the sub-electrode structures) were deposited through shadow masks, also in high vacuum.

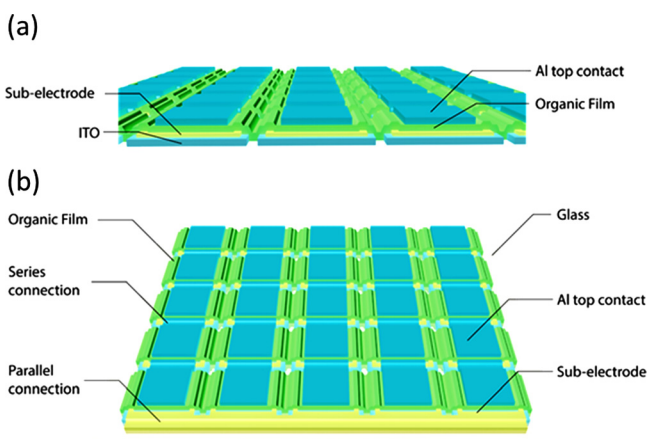

FIG. 4. Views of the OPV module design: (a) Front and (b) top view of the module.

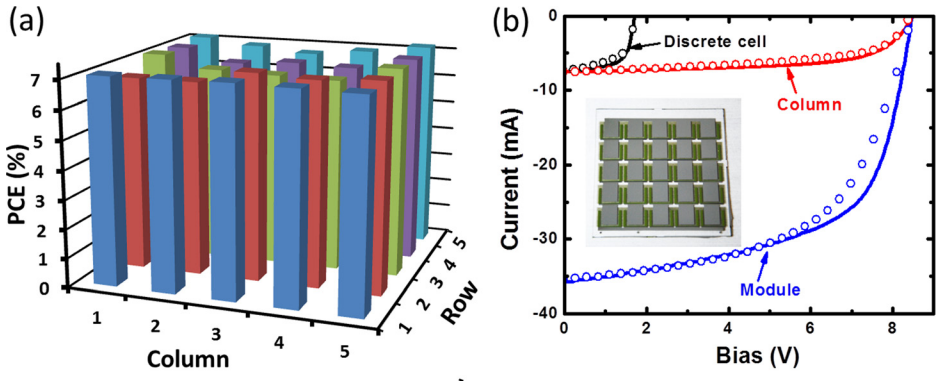

FIG. 5. (a) *PCE* distribution of discrete OPV cells across the module; (b) experimental (circles) and calculated (solid lines) current-voltage (*I-V*) characteristics of a discrete cell (black), a column of 5 cells connected in series (red), and the entire module (blue) under 1 sun illumination. Inset: Photo of the OPV module.

The discrete cell yield is 100%, mainly owing to the snow-cleaning process that efficiently removes particles on the substrate surface, and therefore reduces the risk of shorting. The *PCE* of discrete cells under 1 sun illumination range from 6.7% to 7.2%, with a variation less than 10% across the module as shown in Fig. 5(a).

From Eq. (3), we can write the current-voltage (*I-V*) characteristics in terms of the number of series and parallel cells (S and P, respectively): $I(V) = S\left\{I_s\left[\exp\left(\frac{q\left(\frac{V}{P}-\frac{R_S A I}{S}\right)}{nk_BT}\right)-1\right]-I_{ph}\right\}$. We fit experimental *I-V* curves of a discrete cell, a column of 5 cells and the entire module using Eq. (4), as shown by the lines in Fig. 5(b). For a column of five discrete cells connected in series, the $V_{OC} = 8.45$ V which is within 0.5% of the sum of V_{OC} for 5 individual cells, while the short-circuit current of a column is 7.5 mA, the same as the discrete cell current, as shown in Fig. 5(b). This indicates that resistive losses are minimal in the module compared to that of the individual cells due to a combination of the use of tandem cells, sub-electrode design and circuit layout. The difference between the experimental and fitted *I-V* characteristics for the module (Fig. 5(b)) results from differences in individual device performances likely due to the variation of film thicknesses and contact resistances across the module. Under simulated AM1.5G illumination at one sun intensity, we obtain a module output power of 162 ± 9 mW with $I_{SC} = 36 \pm 1$ mA, $V_{OC} = 8.45 \pm 0.01$ V, and $FF = 53 \pm 1\%$, corresponding to $PCE = 6.5 \pm 0.1\%$, as shown in Fig. 5(b).

In conclusion, we have studied the area-scaling effects of multi-junction OPV cells. Compared to single junction cells, multi-junction cells show a significant reduction in the loss of *PCE* for large compared to small area cells due to higher V_{OC} and lower J_{SC} of the former. This suggests that multi-junction OPV cells can achieve higher efficiency as well as improved scalability when used in practical device applications. Further, in contrast to multi-junction solar cells fabricated using inorganic semiconductors that are made small to reduce cost, multi-junction OPVs actually benefit from scaling to larger sizes. By using sub-electrodes to further reduce the series resistance from the ITO anode, we demonstrated a 25 cm^2 active area organic tandem OPV module with a discrete cell yield of 100% and an efficiency variation of $<10\%$ across the module area.

The authors gratefully acknowledge the financial support in part from the SunShot Next Generation Photovoltaics program of the U.S. Department of Energy (EERE), Award No. DE-EE0005310 (X.X., experiments and analysis; K.L., analysis), and Nano Flex Power Corp. (S.R.F., analysis).

[1]X. Xiao, K. J. Bergemann, J. D. Zimmerman, K. Lee, and S. R. Forrest, Adv. Energy Mater. **4**, 1301557 (2014).
[2]Z. C. He, C. M. Zhong, S. J. Su, M. Xu, H. B. Wu, and Y. Cao, Nat. Photonics **6**, 591 (2012).
[3]X. G. Guo, N. J. Zhou, S. J. Lou, J. Smith, D. B. Tice, J. W. Hennek, R. P. Ortiz, J. T. L. Navarrete, S. Y. Li, J. Strzalka, L. X. Chen, R. P. H. Chang, A. Facchetti, and T. J. Marks, Nat. Photonics **7**, 825 (2013).
[4]J. B. You, L. T. Dou, K. Yoshimura, T. Kato, K. Ohya, T. Moriarty, K. Emery, C. C. Chen, J. Gao, G. Li, and Y. Yang, Nat. Commun. **4**, 1446 (2013).
[5]W. W. Li, A. Furlan, K. H. Hendriks, M. M. Wienk, and R. A. J. Janssen, J. Am. Chem. Soc. **135**, 5529 (2013).
[6]X. Che, X. Xiao, J. D. Zimmerman, D. Fan, and S. R. Forrest, Adv. Energy Mater. **4**, 1400568 (2014).
[7]C. E. Small, S. Chen, J. Subbiah, C. M. Amb, S. W. Tsang, T. H. Lai, J. R. Reynolds, and F. So, Nat. Photonics **6**, 115 (2012).
[8]X. Xiao, J. D. Zimmerman, B. E. Lassiter, K. J. Bergemann, and S. R. Forrest, Appl. Phys. Lett. **102**, 073302 (2013).
[9]X. Xiao, G. D. Wei, S. Y. Wang, J. D. Zimmerman, C. K. Renshaw, M. E. Thompson, and S. R. Forrest, Adv. Mater. **24**, 1956 (2012).
[10]J. D. Zimmerman, B. E. Lassiter, X. Xiao, K. Sun, A. Dolocan, R. Gearba, D. A. Vanden Bout, K. J. Stevenson, P. Wickramasinghe, M. E. Thompson, and S. R. Forrest, ACS Nano **7**, 9268 (2013).
[11]Y. S. Liu, C. C. Chen, Z. R. Hong, J. Gao, Y. Yang, H. P. Zhou, L. T. Dou, G. Li, and Y. Yang, Sci. Rep. **3**, 3356 (2013).
[12]S. Choi, W. J. Potscavage, and B. Kippelen, J. Appl. Phys. **106**, 054507 (2009).
[13]W. I. Jeong, J. Lee, S. Y. Park, J. W. Kang, and J. J. Kim, Adv. Funct. Mater. **21**, 343 (2011).
[14]J. D. Servaites, S. Yeganeh, T. J. Marks, and M. A. Ratner, Adv. Funct. Mater. **20**, 97 (2010).
[15]C. Lungenschmied, G. Dennler, H. Neugebauer, S. N. Sariciftci, M. Glatthaar, T. Meyer, and A. Meyer, Sol. Energy Mater. Sol. Cells **91**, 379 (2007).
[16]A. Manor, E. A. Katz, T. Tromholt, B. Hirsch, and F. C. Krebs, J. Appl. Phys. **109**, 074508 (2011).
[17]A. K. Pandey, J. M. Nunzi, B. Ratier, and A. Moliton, Phys. Lett. A **372**, 1333 (2008).
[18]N. N. Wang, J. D. Zimmerman, X. R. Tong, X. Xiao, J. S. Yu, and S. R. Forrest, Appl. Phys. Lett. **101**, 133901 (2012).
[19]B. E. Lassiter, J. D. Zimmerman, and S. R. Forrest, Appl. Phys. Lett. **103**, 123305 (2013).
[20]N. C. Giebink, G. P. Wiederrecht, M. R. Wasielewski, and S. R. Forrest, Phys. Rev. B **82**, 155305 (2010).
[21]B. P. Rand, D. P. Burk, and S. R. Forrest, Phys. Rev. B **75**, 115327 (2007).
[22]S. Y. Park, W. I. Jeong, D. G. Kim, J. K. Kim, D. C. Lim, J. H. Kim, J. J. Kim, and J. W. Kang, Appl. Phys. Lett. **96**, 173301 (2010).